Localization Based on Parallel Robots Kinematics as an Alternative to Trilateration

Giovanni Garraffa, Antonino Sferlazza, *Member*, *IEEE*, Filippo D'Ippolito, *Member*, *IEEE*, Francesco Alonge, *Senior Member*, *IEEE*

***Abstract*—In this work a new scheme for range-based localization is proposed. The main goal is to estimate the position of a mobile point based on distance measurements from fixed devices, called anchors, and on inertial measurements. Due to the non-linear nature of the problem, an analytic relation to compute the position starting from these measurements does not exist, and often trilateration methods are used, generally based on least-square algorithms. The proposed scheme is based on the modelling of the localization process as a parallel robot, thereby methodologies and control algorithms used in the robotic area can be exploited. In particular, a closed loop control system is designed for tracking the position of a mobile point based on range measurements from fixed anchors, and it is shown a peculiar structure of the tracking error dynamics, whose allows an intuitive gain tuning and ensures global exponential stability. Moreover, it is also shown a nice connection between tuning parameters and rate of convergence of the estimation error. Experimental results confirm the validity of the proposed localization method.**

***Index Terms*—Localization, robots kinematics, range-based measurements, Ultra-Wide Band devices.**

I. Introduction

Navigation and localization of autonomous mobile vehicles represents an important field of research and, for this reason, many efforts have been made in the study of Inertial Navigation Systems (INSs) ([1]–[3]). A crucial point in the INSs is the knowledge of the inertial variables, i.e. position, velocity, acceleration and attitude. In particular, the autonomous vehicles need to know their position and orientation, in order to track a trajectory ([4], [5]) or to cope with general tasks involving navigation and positioning ([6]–[8]). Most INSs are based on 9-Degrees Of Freedom (DOF) Inertial Measurement Unit (IMU). The IMUs are equipped with three accelerometers for measurements of accelerations in the body frame, three gyros for measurement of angular velocity vector referred to the Earth Centered Inertial (ECI) frame, three magnetometers, and a micro-controller for data fusion process.

A common data fusion process for attitude/position estimation, using the IMU, is to employ the strap-down method: first the attitude of the body is computed, then accelerations are projected on an inertial frame and twice integrated to obtain the position [3], [9], [10]. Due to the relevant noise on the accelerometer signals and biases on the gyroscopes, the position computed with the double integration of the projected accelerations is satisfactory only if the observation time is very small. Indeed, position estimation error increases rapidly with time flow, and it depends on the calibration accuracy of the IMU [11]. Since INSs are designed to work on large time window, they cannot rely only on IMU measures. Therefore, to cope with the position estimation problem further data are needed to adjust the estimate.

In order to cope with the above problem, besides the data measured by the IMU, further data are provided by external devices such as Global Positioning System (GPS). With the GPS it is possible to achieve outdoor localization on the Earth as long as satellite signals can be received. A simple sensor fusion method (cf. for example [12]) allows to cope with the different nature and frequency of IMU and GPS measurements, and to obtain a good position estimate. Unfortunately, in indoor scenario or urban environments, there is not the possibility to use GPS because satellite signals cannot be received [13]. For this reason different techniques can be used based on range-measurements [14], [15]. Every range measurement system encompasses a communication system to exchange signal between fixed devices (anchors) and the mobile object to be tracked. The more common range-measurement techniques are Time-of-Flight (ToF) [16], Time Difference-of-Arrival (TDoA) [17] and Received Signal Strength (RSSI) [18]. About the communication system one can use WiFi signals, radio waves, ultrasonic waves, optical laser or Ultra Wide Band (UWB) low power radio signals.

The main problem for localization using range-measurements is to find a relationship between measured distances and position of the mobile object. Due to the intrinsic non-linear nature of the problem this relationship does not exist in a closed form. Position estimation is carried out by means of a geometrical approach called trilateration. To calculate the best approximation of the mobile object position, recursive procedures, generally based on least-square technique, have been explored and proposed in [19]–[21].

In this paper an alternative method to estimate the position of a mobile object, that has never been applied in other past works at best Author's knowledge, is presented. In particular, the main contribution of this paper is to model the range-based localization process as a parallel robot (see for example [22]) and to exploit methodologies and control algorithms used in the robotic area to solve the range-based localization problem. Looking at Fig. 1, if a point P is identified as an

Manuscript received September 10, 2020; revised December 04, 2020; accepted December 26, 2020. *(Corresponding author: Antonino Sferlazza).*

Authors are with the University of Palermo, Department of Engineering, viale delle scienze Ed. 10, 90128 Palermo, Italy (e-mail: giovanni.garraffa01@unipa.it, antonino.sferlazza@unipa.it, filippo.dippolito@unipa.it, francesco.alonge@unipa.it).

end effector, and the distances of this point from the anchors are identified as prismatic links, the system can be interpreted as a parallel robot. Therefore, if the position of the point P has to be determined and the distances from other fixed points are known (or rather the length of the prismatic links is known), this is a classical direct kinematics problem for parallel robot, whose solution does not exists in a closed form. Consequently, the localization problem can be schematized as a control problem which can be formulated as follows: given n measured distances from the point P, determine a control law such that the output variables of the control system, i.e. the observed coordinates of P, generate n feedback distances, computed using the inverse kinematics model, that converge towards the measured ones. When this occurs, the output variables converge towards the coordinate of point P. The principal advantage of this approach is due to the fact that the setup of the localization algorithm can be made using methodologies and control algorithms used in the robotic area.

The approach described in this paper, leading to a closed loop control scheme, can be considered as the counterpart of other methods illustrated in the literature, that use a stochastic framework to design dynamical systems for attitude and position estimation, as the Extended Kalman Filter (EKF) or the Unscented Kalman Filter (UKF). For example, [23] proposes an integrated INS/GNSS system with the aim of enhancing the performance of the navigation system, in terms of reliability and accuracy. In order to construct this system, the INS is modelled by means of two sets of equations, the first one describing the dynamics of position and velocity, and the second one expressing the linearized dynamics of the corresponding errors arising from misalignment sensors, bias and drift in the accelerometers and gyros. A Kalman filter is used as an estimator of these errors that can be used to update the measurements given by the sensors. An other interesting example is given by [24], where the goal is to estimate the heading angle and the attitude of a vehicle using a sliding mode observer. It is designed using a MIMO nonlinear process model not affine with respect to the control variable. The bias vectors of the accelerometers and gyros, are also estimated with the aim of improving the estimate accuracy.

The localization algorithm studied in this paper requires the knowledge of the vehicle attitude for determining the accelerations in the inertial frame from those measured in the body frame, but the attitude problem is not addressed here because extensively treated in the literature (cf. for example [25], [26] and [12]). Indeed, the treatise of the proposed algorithm is independent from the attitude estimation, which is assumed known, and therefore its determination will not be emphasized into the paper. Only some details about the IMU calibration will be given in the experimental set-up description. Instead, the effect of errors introduced by the IMU in the position estimate will be explicitly considered by showing a practical stability of the estimation error, and how the estimation error dynamics can be suitably governed by acting on tuning parameters. Obviously, the proposed scheme could be integrated in a more complex system, where attitude estimation is also considered, to improve the estimation accuracy.

Finally, it is shown in the paper that the estimation error dynamics exhibits a peculiar structure allowing an intuitive tuning and ensuring global exponential stability of the error dynamics. Moreover, it is also shown a nice connection between controller gains and speed of convergence of the estimation error. Note that all these properties cannot be inferred if very complex algorithms are considered. Indeed, in the literature works dealing with the range-based localization, only the stability of the estimation error is proven, but its *"exact"* dynamics in terms of speed of convergence, steady-state errors, etc., is not explicitly considered.

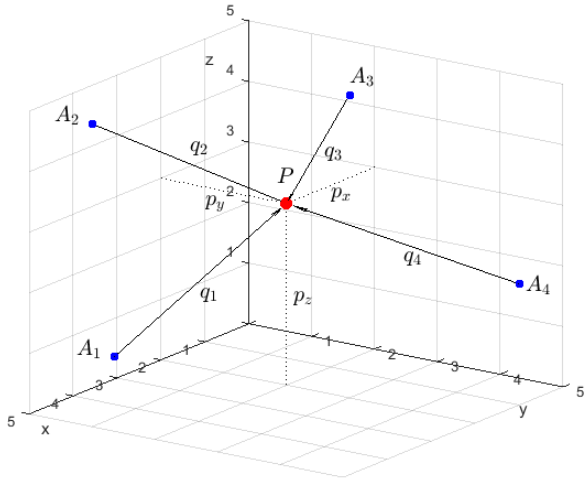

Fig. 1. Scheme of the localization system.

Experimental results will show the effectiveness of the proposed approach.

Notation: $\mathbb{R}^n$ denotes the n-dimensional Euclidean space. $\mathbb{R}_{\geq 0}$ denotes the set of nonnegative real numbers. $\mathbf{I}_q$ denotes the identity matrix of order $q \in \mathbb{Z}_{\geq 0}$. $\lambda_m(S)$ and $\lambda_M(S)$ denote, respectively, the minimum and the maximum eigenvalues of a positive definite symmetric matrix S. $|x|$ denotes the Euclidean norm of a vector $x \in \mathbb{R}^n$. Symbol $\otimes$ denotes the Kronecker product.

II. Problem Statement

The goal of this paper is the position estimation of mobile vehicles in the 3-D space, starting from range measurements coming from fixed anchors whose positions are known. In particular, Fig. 1 schematizes a possible context where the position coordinates (p_x, p_y and p_z) of a mobile point P in a 3-D space have to be estimated by measuring the distances, $q_1, \cdots, q_n$, from n anchors located in fixed points, $A_1, \cdots, A_n$. This problem is not new, and there is a huge number of works in literature dealing with it. However, as shown in the Introduction, most of them calculate the best approximation of the mobile object position by recursive procedures, generally based on least-square techniques, by using a geometrical approach called trilateration. This is because, due to both the intrinsic non-linear nature of the problem and the disturbances affecting the distance measurements, it is difficult to determine a closed-form solution for the position of P.

In this paper a novel method to estimate the mobile object position P, that has never been applied in other past works

at best Author's knowledge, is presented. In particular, the direct kinematics algorithm for parallel robot will be used. The inverse kinematics equations establish the relationship between the end-effector position and the joint variables of a parallel robot by means of a closed form solution. Note that for serial robot it is exactly the opposite, i.e. direct kinematics (from the joint variables to the end-effector) has always a unique closed form solution, contrary to the inverse kinematics problem.

Looking at Fig. 1, if the point P is identified as an end effector, and the distances q_1, q_2, q_3 and q_4 as prismatic links, the localization process can be interpreted as a parallel robot. Therefore, if the position of the point P is known and distances q_1, q_2, q_3 and q_4 have to be obtained, this is a classical inverse kinematics problem for parallel robot, whose solution always exists in a closed form. However, the goal is the opposite, or rather to determine the position of the point P starting from the measurements of the distances q_1, q_2, q_3 and q_4. For this reason it is possible to take advantage from the results already presented in the robotic literature context (see [22]), where this problem has been addressed, and to extend these results for the presented purpose.

A further important consideration is that the minimum number of anchors which allows to obtain the position of P without indeterminacy, is equal to four. Indeed, the use of three anchors causes indeterminacy in the position of P, because of it could be either over or under the anchors' plane, or rather the plane containing the three anchors. However, this indeterminacy can be excluded if it is known, a priory, that the motion of P occurs either under or over the anchors' plane.

III. Estimation algorithm

As already said in the precedent Section, looking at Fig. 1, if the point P is identified as an end effector, and the distances q_1, q_2, q_3 and q_4 as prismatic links, the localization process can be interpreted as a parallel robot whose direct kinematics equations are given by ([27, Chapter 3.7]):

$$\mathbf{p} = \mathcal{K}(\mathbf{q}). \tag{1}$$

However, in the case under study, it is known the structure of the inverse kinematics, given by:

$$\mathbf{q} = \mathcal{K}^{-1}(\mathbf{p}), \tag{2}$$

where the generic component q_i, $i=1,...,n$, is given by:

$$q_i = \sqrt{(x_i - p_x)^2 + (y_i - p_y)^2 + (z_i - p_z)^2} \quad \forall i \in \mathcal{S}, \tag{3}$$

where x_i, y_i, z_i denote the components of the position of the i^{th} anchor A_i referred to a fixed reference frame, p_x, p_y and p_z, denote the coordinates of the mobile point P, q_i is the distance between P and the i^{th} anchor and $\mathcal{S} = \{1, 2, \cdots n\}$ denotes a discrete set of integer numbers. In the case under study, $n \geq 3$.

The problem to solve is to estimate the coordinates of P, thus determining the direct kinematics (1). To this end, by computing the time derivative of equation (2), it is obtained:

$$\dot{\mathbf{q}} = \mathbf{J}_{\mathcal{K}^{-1}}(\mathbf{p})\dot{\mathbf{p}}, \tag{4}$$

where $\mathbf{J}_{\mathcal{K}^{-1}}(\mathbf{p}) \in R^{n\times 3}$ is the Jacobian matrix of the vectorial function $\mathcal{K}^{-1}(\mathbf{p})$, given by:

$$\mathbf{J}_{\mathcal{K}^{-1}}(\mathbf{p}) = \frac{\partial \mathcal{K}^{-1}(\mathbf{p})}{\partial \mathbf{p}}. \tag{5}$$

Computing the derivative of equation (1), it is obtained:

$$\dot{\mathbf{p}} = \mathbf{J}_{\mathcal{K}}(\mathbf{q})\dot{\mathbf{q}}, \tag{6}$$

where:

$$\mathbf{J}_{\mathcal{K}}(\mathbf{q}) = \frac{\partial \mathcal{K}(\mathbf{q})}{\partial \mathbf{q}}. \tag{7}$$

From (6) and (4), it is obtained $\mathbf{J}_{\mathcal{K}}(\mathbf{q})\mathbf{J}_{\mathcal{K}^{-1}}(\mathbf{p}) = \mathbf{I}_3$, and consequently $\mathbf{J}_{\mathcal{K}}(\mathbf{q})$ is the left pseudoinverse matrix of $\mathbf{J}_{\mathcal{K}^{-1}}(\mathbf{p})$, given by:

$$\mathbf{J}_{\mathcal{K}}(\mathbf{q}) = (\mathbf{J}^T_{\mathcal{K}^{-1}}(\mathbf{p})\ \mathbf{J}_{\mathcal{K}^{-1}}(\mathbf{p}))^{-1}\mathbf{J}_{\mathcal{K}^{-1}}{}^T(\mathbf{p}). \tag{8}$$

Now it is possible to use the inverse kinematics algorithm shown in [27, Chapter 3.7], but instead to apply the algorithm to robots, here it is applied in the different context of the localization. Additionally, differently than [27, Chapter 3.7], where a fixed end effector position is considered, here the case of a mobile point is addressed, by exploiting inertial measurements (usually provided by IMU) for improving the position estimation.

In the following the case when the anchor number n is equal to three ($n = 3$) is considered, with respect to the case $n \geq 4$, since for $n = 3$ it is possible to show some interesting properties of the estimation error dynamics, that allow to give some intuitive tuning hints for the estimator design.

A. Localization using three anchors

Before to give the main results of this subsection, the following Assumption is provided:

Assumption 1: Given three anchors A_1, A_2 and A_3, identifying with Σ_A the plane containing these anchors, if an orthonormal reference frame x-y-z is fixed, whose x and y axis belong to Σ_A, the sign of the z component of the point P, with respect to the x-y-z reference frame, is assumed known.

Note that Assumption 1 is compliant with the consideration given in Section II about the minimum number of anchors which allows to obtain a unique solution.

The structure of the proposed closed loop control system for estimating $\mathbf{p}$ is given in Fig. 2, where the controller is described by the following equation:

$$\dot{\hat{\mathbf{p}}} = \mathbf{J}^{-1}_{\mathcal{K}^{-1}}(\hat{\mathbf{p}}) \left(\dot{\mathbf{q}} + \mathbf{K}_P(\mathbf{q} - \hat{\mathbf{q}}) + \mathbf{K}_I \int_0^t (\mathbf{q} - \hat{\mathbf{q}}) d\tau \right). \tag{9}$$

where $\hat{\mathbf{p}}$ and $\hat{\mathbf{q}}$ are respectively the estimate of the position and distance vectors, whereas $\mathbf{p}$ and $\mathbf{q}$ are the true position and distance vectors. Note that the controller (9) is well defined because $\mathbf{J}^{-1}_{\mathcal{K}^{-1}}$ there exists, since $\mathbf{J}_{\mathcal{K}^{-1}}$ is a square full-rank matrix except the case when the point P coincides with one of the anchors. However, this last condition is not realistic from practical point of view, and therefore it will not be addressed.

One result of this work proves stability and convergence of the estimation error in the extended error space corresponding to the error variables:

$$\mathbf{e} = \begin{bmatrix} \mathbf{e}_q \\ \mathbf{e}_p \end{bmatrix} = \begin{bmatrix} \mathbf{q} - \hat{\mathbf{q}} \\ \mathbf{p} - \hat{\mathbf{p}} \end{bmatrix}. \tag{10}$$

Now it is possible to give the following theorem.

Theorem 1: If Assumption 1 holds, the estimation errors (10) converge exponentially to zero along dynamics (9) and (6) if and only if there exist matrices $\mathbf{K}_P$ and $\mathbf{K}_I$ such that matrix $\mathbf{\Gamma}$, defined as:

$$\mathbf{\Gamma} = \begin{bmatrix} \mathbf{0} & \mathbf{I} \\ -\mathbf{K}_I & -\mathbf{K}_P \end{bmatrix}, \tag{11}$$

is Hurwitz.

Proof: Premultiplying both members of (9) by $\mathbf{J}_{\mathcal{K}^{-1}}(\hat{\mathbf{p}})$, and considering equation (4), it is obtained:

$$\dot{\hat{\mathbf{q}}} = \dot{\mathbf{q}} + \mathbf{K}_P(\mathbf{q} - \hat{\mathbf{q}}) + \mathbf{K}_I \int_0^t (\mathbf{q} - \hat{\mathbf{q}}) d\tau. \tag{12}$$

Since $\mathbf{e}_q = \mathbf{q} - \hat{\mathbf{q}}$, equation (12) can be rewritten as:

$$\dot{\mathbf{e}}_q + \mathbf{K}_P \mathbf{e}_q + \mathbf{K}_I \int_0^t (\mathbf{e}_q) d\tau = 0. \tag{13}$$

By deriving (13) it is obtained:

$$\ddot{\mathbf{e}}_q + \mathbf{K}_P \dot{\mathbf{e}}_q + \mathbf{K}_I \mathbf{e}_q = 0. \tag{14}$$

Therefore if matrix (11) is Hurwitz, then tracking error $\mathbf{e}_q$ converges exponentially to zero.

In order to prove the exponential convergence of the estimation error in the extended error space (10), it is necessary to show that also $\mathbf{e}_p$ converges exponentially to zero. Based on straightforward geometric considerations, in case of three anchors, Eq. (1) has two solutions, but only one can be chosen under Assumption 1. Therefore, the position error can be written as:

$$\mathbf{e}_p = \mathcal{K}(\mathbf{q}) - \mathcal{K}(\hat{\mathbf{q}}). \tag{15}$$

Since $\mathbf{e}_q$ converges exponentially to zero (as above proven), this implies that $\hat{\mathbf{q}} \to \mathbf{q}$ and therefore $\mathcal{K}(\mathbf{q}) - \mathcal{K}(\hat{\mathbf{q}}) \to 0$. This consideration leads to the exponential convergence of estimation error in the extended error space (10), because both $\mathbf{e}_q$ and $\mathbf{e}_p$ converge exponentially to zero. Note that, Assumption 1 can be removed if more than three anchors are used, because in this case Eq. (1) admits only one solution.

Finally, to prove also necessity, it is assumed that matrix $\mathbf{\Gamma}$ is not Hurwitz. This implies that at least one eigenvalue is with positive real part. This clearly generates a solution of (14) not converging to zero, thus proving that the exponential convergence of estimation error does not hold. □

Remark 1: Note that the role of the IMU in the algorithm is in the computation of the term $\dot{\mathbf{q}}$ in (9). Indeed it is computed applying (4) where $\dot{\mathbf{p}}$ is obtained by integration of the acceleration measured by the IMU. The reason of adding this term is because fast transients can be better tracked compared with the case when the inertial measurements are not considered. However, this term $\dot{\mathbf{q}}$ in (9) is usually affected by errors because IMU measurements are noisy and biased. Moreover, in the calculation of $\dot{\mathbf{q}}$, $\mathbf{J}_{\mathcal{K}^{-1}}(\hat{\mathbf{p}})$ is used instead of $\mathbf{J}_{\mathcal{K}^{-1}}(\mathbf{p})$, therefore, this approximation represents a second source of error for the term $\dot{\mathbf{q}}$. However, as it will be shown in Section III-B, due to the continuity property of the Jacobian this error is bounded. In this case, by following the same approach of Theorem 1 it is possible to show a practical stability of the estimation error when $\dot{\mathbf{q}}$ in (9) is not perfectly known. Indeed, assuming $\dot{\tilde{\mathbf{q}}} := \dot{\mathbf{q}} + \mathbf{\Delta}_{\dot{\mathbf{q}}}$, where $\dot{\tilde{\mathbf{q}}}$ is the measured quantity and $\Delta_{\dot{\mathbf{q}}}$ is the related bounded error, and replacing $\dot{\tilde{\mathbf{q}}}$ in (9) instead of $\dot{\mathbf{q}}$, then (14) can be rewritten as:

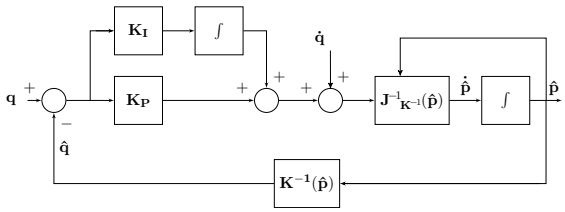

Fig. 2. Block diagram of the proposed algorithm.

$$\ddot{\mathbf{e}}_q + \mathbf{K}_P \dot{\mathbf{e}}_q + \mathbf{K}_I \mathbf{e}_q + \Delta_{\dot{\mathbf{q}}} = 0. \tag{16}$$

Equation (16) leads to a steady state-error equal to:

$$\begin{bmatrix} \|\mathbf{e}_q\|_{ss} \\ \|\dot{\mathbf{e}}_q\|_{ss} \end{bmatrix} = \begin{bmatrix} \frac{\|\Delta_{\dot{\mathbf{q}}}\|}{\|\mathbf{K}_I\|} \\ 0 \end{bmatrix}. \tag{17}$$

Equation (17) highlights that possible measurement errors on $\dot{\mathbf{q}}$ can be suitably reduced by increasing $\mathbf{K}_I$.

Remark 2: Note that the proposed controller (9) can be simplified by neglecting the integral term, and considering the following simplified equation:

$$\dot{\hat{\mathbf{p}}} = \mathbf{J}^{-1}_{\mathcal{K}^{-1}}(\hat{\mathbf{p}}) \left(\dot{\mathbf{q}} + \mathbf{K}_P(\mathbf{q} - \hat{\mathbf{q}}) \right). \tag{18}$$

However, as shown in Remark 1, the integral action gives an important contribution for reducing the estimation error when $\dot{\mathbf{q}}$ is not perfectly known.

Note that the structure of the controller (9) is nonlinear, and it is suitably chosen so that the dynamics of the tracking error, defined in (10), becomes linear and time-invariant, as shown in (13) and (14). Therefore, it is not necessary a linearization procedure as it has been done in other past works [23].

In the following, an appealing result from the practical point of view is given. In particular, an explicit tuning rule is given to determine parameters $\mathbf{K}_P$ and $\mathbf{K}_I$ in order to ensure a well defined convergence speed of the tracking error $\mathbf{e}_q$ and, consequently, of the estimation error $\mathbf{e}_p$.

Proposition 1: Given scalars $\alpha > 0$ and $\beta > 2$, if $\mathbf{K}_P := k_p \otimes \mathbf{I}_3 = \beta\alpha \otimes \mathbf{I}_3$ and $\mathbf{K}_I := k_i \otimes \mathbf{I}_3 > \alpha^2(\beta - 1) \otimes \mathbf{I}_3$, there exist a symmetric positive-definite matrix $\mathbf{P} := \mathbf{I}_3 \otimes \overline{\mathbf{P}}$ with $\overline{\mathbf{P}} \in \mathbb{R}^{2\times 2}$, such that:

$$|\overline{\mathbf{e}}_q(t)| \leq \sqrt{k} \mathrm{e}^{-\alpha t} |\overline{\mathbf{e}}_q(0)|, \quad \forall t \geq 0, \tag{19}$$

where $\overline{\mathbf{e}}_q := [\mathbf{e}_q^\top, \dot{\mathbf{e}}_q^\top]^\top$ and $k = \frac{\lambda_m(\mathbf{P})}{\lambda_M(\mathbf{P})}$.

Proof. Consider the radially unbounded Lyapunov function defined as:

$$V(\overline{\mathbf{e}}_q) := \overline{\mathbf{e}}_q^\top \mathbf{P} \overline{\mathbf{e}}_q, \tag{20}$$

where $\mathbf{P}$ is a symmetric positive-definite matrix, whose derivative is:

$$\dot{V}(\overline{\mathbf{e}}_q) = \overline{\mathbf{e}}_q^\top (\mathbf{P}\boldsymbol{\Gamma} + \boldsymbol{\Gamma}^\top \mathbf{P})\overline{\mathbf{e}}_q, \tag{21}$$

where $\boldsymbol{\Gamma}$ is defined in (11). For [28, Definition 8.1] and [28, Theorem 8.2] the bound in (19) on $\overline{\mathbf{e}}_q$ can be inferred if matrix $\mathbf{P}$ in (21) is such that:

$$\mathbf{P}\boldsymbol{\Gamma} + \boldsymbol{\Gamma}^\top \mathbf{P} < -2\alpha \mathbf{P}. \tag{22}$$

In order to verify matrix inequality in (22) it needs to be:

$$\mathbf{P}\boldsymbol{\Gamma} + \boldsymbol{\Gamma}^\top \mathbf{P} + 2\alpha \mathbf{P} = \mathbf{P}(\boldsymbol{\Gamma} + \alpha \mathbf{I}_6) + (\boldsymbol{\Gamma} + \alpha \mathbf{I}_6)^\top \mathbf{P} < 0. \tag{23}$$

By defining $\mathbf{K}_P := k_p \otimes \mathbf{I}_3$ and $\mathbf{K}_I := k_i \otimes \mathbf{I}_3$ and applying the property of the Kronecker product, (23) can be rewritten as:

$$\begin{aligned} \left(\mathbf{I}_3 \otimes \overline{\mathbf{P}}\right)\left(\mathbf{I}_3 \otimes \boldsymbol{\Gamma}_\alpha\right) + \left(\mathbf{I}_3 \otimes \boldsymbol{\Gamma}_\alpha\right)^\top \left(\mathbf{I}_3 \otimes \overline{\mathbf{P}}\right) = \\ = \mathbf{I}_3 \otimes \left(\overline{\mathbf{P}}\boldsymbol{\Gamma}_\alpha + \boldsymbol{\Gamma}_\alpha^\top \overline{\mathbf{P}}\right) < 0, \end{aligned} \tag{24}$$

where $\boldsymbol{\Gamma}_\alpha = \left[\begin{smallmatrix} \alpha & 1 \\ -k_i & -k_p+\alpha \end{smallmatrix}\right] \in \mathbb{R}^{2\times 2}$. Since $\mathbf{I}_3 > 0$, there always exist $\overline{\mathbf{P}}$ satisfying (24) if $\boldsymbol{\Gamma}_\alpha$ is Hurwitz [28, Theorem 8.3], or rather $\boldsymbol{\Gamma}_\alpha$ has eigenvalues with negative real part. If k_p and k_i are defined as in the statement:

$$\begin{cases} k_p = \beta\alpha, \\ k_i > \alpha^2(\beta - 1), \end{cases} \tag{25}$$

with $\beta > 2$, then the polynomial defined as $\det(\lambda \mathbf{I}_2 - \boldsymbol{\Gamma}_\alpha) = \lambda^2 + \lambda(k_p - 2\alpha) + \alpha(\alpha - k_p) + k_i$ has roots with negative real part, which in turn implies that $\boldsymbol{\Gamma}_\alpha$ is Hurwitz and therefore there always exist $\overline{\mathbf{P}}$ satisfying (24). Finally, the existence of $\overline{\mathbf{P}}$ implies also the existence of $\mathbf{P} = \mathbf{I_3} \otimes \overline{\mathbf{P}}$ such that (22) is satisfied. This concludes the proof. □

Note that (19) induces an exponential bound with rate of convergence equal to α. Therefore α can be considered the rate of convergence for the tracking error $\overline{\mathbf{e}}_q$.

Remark 3: To obtain $\overline{\mathbf{P}}$ and k in (19), the following numerical problem can be solved by means of YALMIP [29]:

$$\begin{aligned} \min_{k, \overline{\mathbf{P}} = \overline{\mathbf{P}}^\top} k, \quad \text{subject to:} \\ \overline{\mathbf{P}}\boldsymbol{\Gamma}_\alpha + \boldsymbol{\Gamma}_\alpha^\top \overline{\mathbf{P}} \le -2\alpha \overline{\mathbf{P}}, \\ \mathbf{I}_2 \le \overline{\mathbf{P}} \le k \mathbf{I}_2, \end{aligned} \tag{26}$$

where α is the desired speed of convergence and $\boldsymbol{\Gamma}_\alpha = \left[\begin{smallmatrix} \alpha & 1 \\ \alpha^2(1-\beta) - \eta & \alpha(1-\beta) \end{smallmatrix}\right]$ with $\eta > 0$ and $\beta > 2$.

B. Localization using more than three anchors

If a number of anchors $n > 3$ is used, generalization of (9) allows to obtain a solution based on the pseudo-inverse of the Jacobian matrix. Generalized formulation of the estimation algorithm leads to the following controller:

$$\dot{\hat{\mathbf{p}}} = \mathbf{J}^{\#}_{\mathcal{K}^{-1}}(\hat{\mathbf{p}}) \left(\dot{\mathbf{q}} + \mathbf{K}_P(\mathbf{q} - \hat{\mathbf{q}}) + \mathbf{K}_I \int_0^t (\mathbf{q} - \hat{\mathbf{q}}) d\tau \right), \tag{27}$$

where $\mathbf{J}^{\#}_{\mathcal{K}^{-1}}(\hat{\mathbf{p}})$ is the left pseudoinverse of the Jacobian matrix and it is defined as:

$$\mathbf{J}^{\#}_{\mathcal{K}^{-1}}(\hat{\mathbf{p}}) = \left(\mathbf{J}^\top_{\mathcal{K}^{-1}}(\hat{\mathbf{p}}) \mathbf{J}_{\mathcal{K}^{-1}}(\hat{\mathbf{p}})\right)^{-1} \mathbf{J}^\top_{\mathcal{K}^{-1}}(\hat{\mathbf{p}}). \tag{28}$$

The theoretical results already given for the case when $n = 3$ can be extended to the case of $n > 3$ since the structure of the controller is the same. Here they are highlighted some properties of the Jacobian matrix of the vectorial function $\mathcal{K}^{-1}(\mathbf{p})$, already defined in (5), whose explicit form is:

$$\mathbf{J}_{\mathcal{K}^{-1}}(\mathbf{p}) = - \begin{bmatrix} j_{1x} & j_{1y} & j_{1z} \\ j_{2x} & j_{2y} & j_{2z} \\ \vdots & \vdots & \vdots \\ j_{nx} & j_{ny} & j_{nz} \end{bmatrix} \in \mathbb{R}^{n \times 3} \tag{29}$$

where:

$$j_{ix} = \frac{x_i - p_x}{q_i}, \; j_{iy} = \frac{y_i - p_y}{q_i}, \; j_{iz} = \frac{z_i - p_z}{q_i}, \; i = 1, 2, \ldots, n.$$

The elements of $\mathbf{J}_{\mathcal{K}^{-1}}(\mathbf{p})$ are continuos function of $\mathbf{p}$ except when $q_i = 0$. This may happens if the point $\mathbf{p}$ coincide with one of the n anchors, anyway, as already discussed in Section III-A, this condition is not realistic from a practical point of view, and it will not be addressed. Therefore, it is considered: $\mathbf{p} \in \boldsymbol{\Omega}$ with $\boldsymbol{\Omega} = \mathbb{R}^3 \backslash \{\mathbf{A_1} \cup \mathbf{A_2} \cup \cdots \cup \mathbf{A_n}\}$.

The continuity of the elements of the Jacobian $\mathbf{J}_{\mathcal{K}^{-1}}(\mathbf{p})$ in a generic point $\mathbf{p} \in \boldsymbol{\Omega}$ implies that $\forall \epsilon > 0$ there exist a neighborhood of $\mathbf{p}$ of radius δ such that if $\|\hat{\mathbf{p}} - \mathbf{p}\| < \delta$, then $\|\mathbf{J}_{\mathcal{K}^{-1}}(\hat{\mathbf{p}}) - \mathbf{J}_{\mathcal{K}^{-1}}(\mathbf{p})\| < \epsilon$, which means that $\mathbf{J}_{\mathcal{K}^{-1}}(\hat{\mathbf{p}})$ can be approximated by $\mathbf{J}_{\mathcal{K}^{-1}}(\mathbf{p})$ and vice versa. Note that the continuity property is also uniform because of the above mentioned elements of the Jacobian $\mathbf{J}_{\mathcal{K}^{-1}}(\hat{\mathbf{p}})$ are continuous functions in each point of the space where they are defined. This property of the Jacobian ensures that the proposed estimation solution is well posed.

Remark 4: Note that, if a number of anchors greater than 3 is used, there is not indetermination in the sign of the z component of $\mathbf{p}$, because more information are available for the estimation algorithm. Therefore Assumption 1 is no longer necessary. The effectiveness of the control law (27) will be shown in the experimental result Section.

IV. Experimental Set-Up

A test setup has been suitably built to experimentally verify the proposed localization algorithm. The employed test setup consists of:

1) *Localization system*: it is composed by four fixed beacons placed on the testing scene and a mobile beacon mounted on the object to be tracked.
2) *IMU*: it includes gyroscope, accelerometer and magnetometer sensor.
3) *Processing unit*: it consists of a Raspberry Single Board Computer with Wifi connection.
4) *Reference system*: it is a 6-axes industrial robot system.

Figure 3 shows a photo of the experimental setup.

Localization System. As explained above, this system is composed by four fixed devices placed on the scene and a mobile device placed on the object to be tracked. The beacon hardware is based on DW1000 IC from Decawave, a single chip IEEE802.15.4-2011UWB compliant device with internal high precision counter (each LSB of the timestamp timer is 15.65 pS that leads to maximum theoretical accuracy of ±5mm) for Time-of-Flight (ToF) measurement.

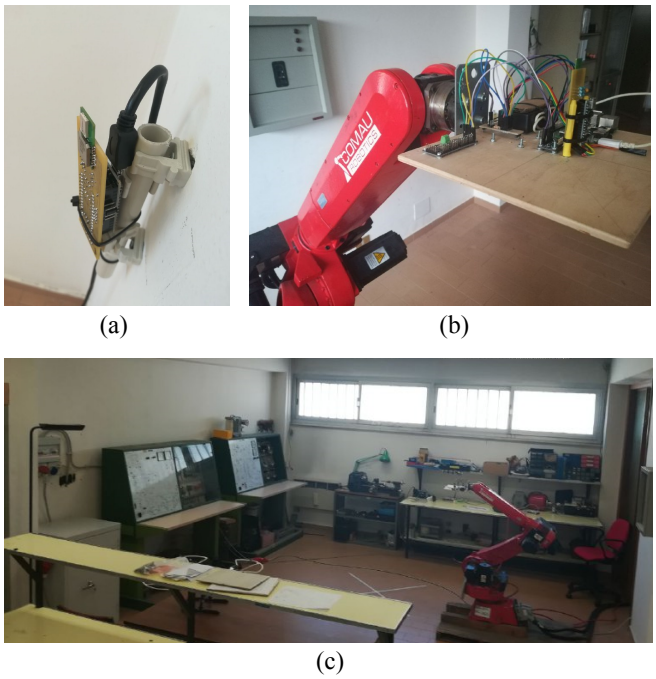

Fig. 3. Photo of the experimental setup: (a) fixed beacon, (b) mobile plate to be tracked, (c) indoor scenario.

Since a two-way ranging technique has been used to perform ToF measures, more time captures are needed to compute a single distance measurement. This lead to a measurement accuracy, as indicated on the DW1000 manufacturer website, of $\pm$10cm instead of the maximum theoretical accuracy of $\pm$5mm. Moreover, each beacon is equipped with external Atmel microcontroller. The range measurement system has an actual equivalent refresh rate up to 12Hz.

IMU. It consists of a LSM9DS1, a ST-Microelectronics chip that integrate 3 acceleration channels, 3 angular rate channels and 3 magnetic field channels with MEMS technology. The ST-Microelectronics data-sheet gives $\pm 2g$ as linear acceleration full scale, $\pm$4G as full scale for the magnetic field and ± 245 degree-per-seconds as angular rate full scale for the gyroscope. About the sensitivity, it is reported to be 0.061mg/LSB for the accelerometer, 0.14 mG/LSB for the magnetometer and 8.75 mdps/LSB for the gyroscope at 25°C.

With regards to IMU calibration, the following methods have been used. For the accelerometer the on-the-field method based on Gauss-Newton nonlinear optimization given in [30] has been used to compute bias and scale factor for each axis and the cross-axis symmetrical factors. For the magnetometer, the ellipsoid fitting method given in [31] has been used to perform the sensor calibration. Finally, to obtain the gyroscope bias, each of the three gyroscope axis measurements has been integrated (when the IMU is still) for one minute and then the mean value has been calculated. This mean value is assumed as initial value for the bias. Subsequently, the fusion algorithm from [32], used to perform the attitude estimation, also computes online gyroscope bias drift compensation. For more details the reader is addressed to [30]–[32].

Processing Unit. It consists of a Raspberry Pi3 core that runs

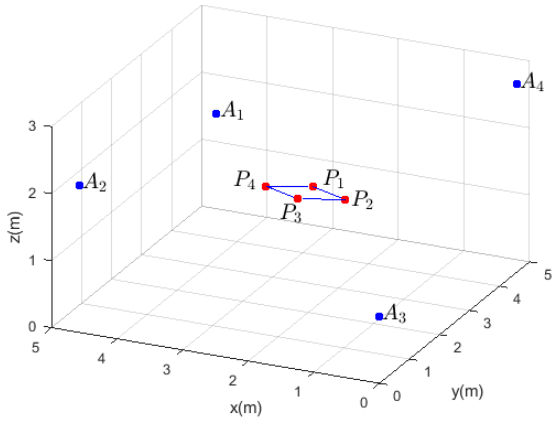

Fig. 4. Scheme of the experimental test: (A_i) fixed beacon, (P_i) points of the rhombus path.

compiled C code generated from Matlab/Simulink coder, with a 100Hz sampling frequency. Raspberry Pi3 is based on an ARM Cortex-A53, a 4-cpu 64bit processor running at 1.2GHz. It can communicate with a I2C bus and a Wifi connection.

Reference System. All the above listed components, except for fixed beacons, are placed on a plate that is fixed on the end effector of a Smart Six-1.4 industrial robot Comau. It is an anthropomorphic robot with 6 DoF. Imposing a trajectory on the scene, it is used as *"reference"* for algorithms quality evaluation. The robot is equipped with C4G controller, which can communicate with the Processing Unit, through wireless UDP protocol. The information shared with the processing unit are position and attitude of the plate where the measurement unit is fixed. Moreover, with reference to the positioning of the IMU on the plate rigidly connected to the robot, the alignment is carried out so that roll, pitch and yaw angles are zero.

The experimental implementation has been carried out by means of Matlab/Simulink. In particular, the Raspberry runs a pre-compiled C code built from the Simulink scheme of the proposed algorithm. Real time execution, in external mode, has a frequency of 100Hz. UWB and IMU devices are connected to the Raspberry by mean of I2C digital Bus. I2C and LSM9DS1 Simulink blocks are used for interfacing the sensor measurements with the Simulink scheme of the controller.

V. Experimental Results

The experimental test consists of a path with a rhombus shape like in Fig. 4. In particular, the robot is actuated so that the plate, mounted on its end effector, tracks a rhombus whose the major diagonal is oriented like the x-axis and it is 1.1 meters long, while the minor diagonal is 0.5 meters long. The starting point of the rhombus is $p_{1(x,y,z)} = [2.02, 2.2, 1.8]$, next point is $p_{2(x,y,z)} = [1.42, 1.95, 1.8]$, then $p_{3(x,y,z)} = [2.02, 1.70, 1.80]$, $p_{4(x,y,z)} = [2.62, 1.95, 1.8]$ and finally it returns to the initial position. Four fixed anchors are placed in $A_{1(x,y,z)} = [4.58, 4.58, 1.6]$, $A_{2(x,y,z)} = [4.58, 0, 2.2]$, $A_{3(x,y,z)} = [0, 0, 1]$ and $A_{4(x,y,z)} = [0, 4.58, 2.8]$. In order to highlight the convergence transient of the estimation error for the proposed algorithm, the initial condition has been set far

from the real one and, in particular, in $p_{0(x,y,z)} = [0, 0, 1.8]$. Finally, to test only the closed loop localization algorithm proposed in this paper, the motion imposed to the end effector is chosen so that the corresponding Euler angles are equal to zero. In this way, the results obtained are independent of attitude errors produced by the IMU because the attitude is known and the acceleration measurements referred to the body frame correspond to that ones referred to the inertial frame.

To prove the effectiveness of the proposed algorithm two tests have been carried out, the first one using 3 anchors whose results are shown in Section V-A and the second one using 4 anchors whose results are shown in Section V-B. Each test was performed selecting $k_p = 2$ and $k_i = 1$, that correspond with a convergence rate $\alpha = 1$ according to Proposition 1. Also some tests with different value of α have been carried out in order to validate the exponential bound (19) of Proposition 1.

A. Experimental results using three anchors

In this first test only distance measurements from anchors A_1, A_2 and A_3 have been used in order to prove the proposed estimation algorithm given in (18). In Figs. 5-6 the waveforms of the position components p_x and p_y are shown as well as the corresponding estimation error e_{px} and e_{py}. The measured and estimated distances from anchors q_1, q_2 and q_3 are shown in Fig. 7, while in Fig. 8 there are the corresponding estimation errors e_{q1}, e_{q2} and e_{q3}. Finally in Fig. 9 it is shown a comparison of the three distance estimation error waveforms e_{q1}, e_{q2} and e_{q3} obtained with three different values of α to prove the validity of the exponential bound (19). Starting from a different initial condition, it is evident that the feedback variables, i.e. the estimated distances, converge to the reference values and the control system tracks correctly the path providing a good position estimate, indeed the estimated variables exponentially converge to the corresponding true variables. The steady state errors have zero mean, both for positions and distances and they are contained in a band of ± 0.05 m for positions and ± 0.1 m for distances, coherently with the accuracy of the sensors. Moreover, the validity of the exponential bound (19) of Proposition 1 has been proven, as clearly shown in Fig. 9.

B. Experimental results using four anchors

In this second test distance measurements from all anchors A_1, A_2, A_3 and A_4 have been used in order to prove the proposed estimation algorithm given in (27). In Figs. 10-11 the waveforms of the position components p_x and p_y are shown as well as the corresponding estimation errors e_{px} and e_{py}. The measured and estimated distances from anchors q_1, q_2, q_3 and q_4 are shown in Fig. 12, while in Fig. 13 there are the corresponding distance estimation errors e_{q1}, e_{q2}, e_{q3} and e_{q4}. Finally, in Fig. 14 a comparison is shown among distance estimation errors obtained with three different values of α to prove the validity of the exponential bound (19).

In this case of four anchors, similar results of the case with three anchors have been obtained and therefore similar comments to those above given can be inferred. This shows the effectiveness of the proposed approach and the correctness of the theoretical results shown in Section III.

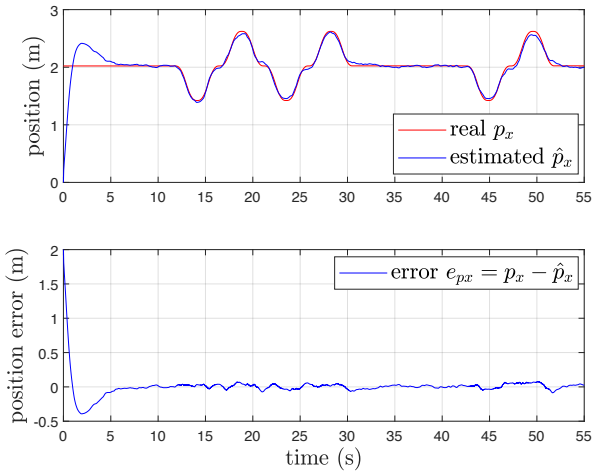

Fig. 5. Real and estimated position component p_x. Test with 3 anchors.

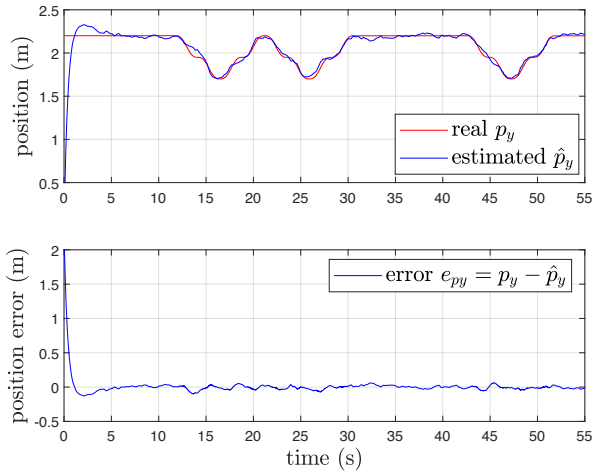

Fig. 6. Real and estimated position component p_y. Test with 3 anchors.

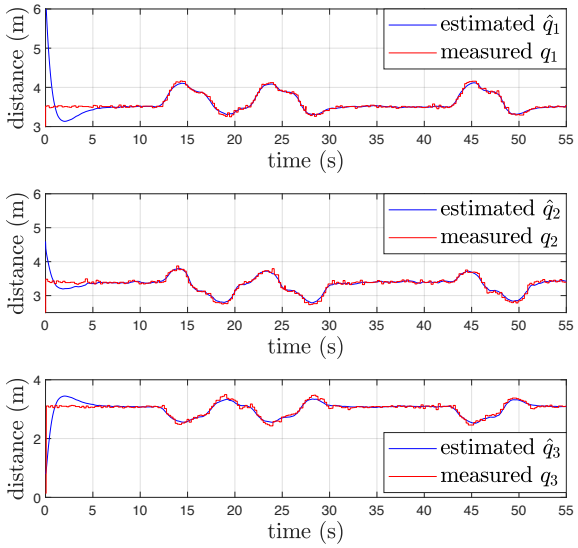

Fig. 7. Measured and estimated distances q_1,q_2 and q_3. Test with 3 anchors.

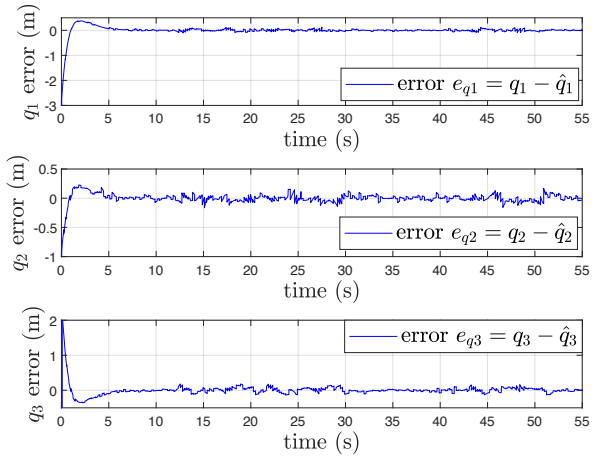

Fig. 8. Distance errors. Test with 3 anchors.

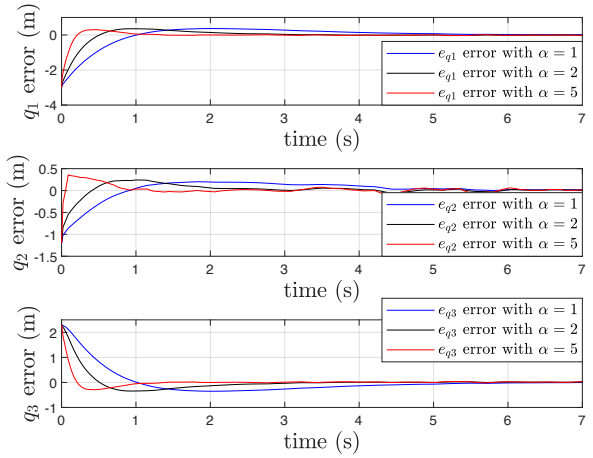

Fig. 9. Estimation error waveforms with different values of α. Test with 3 anchors.

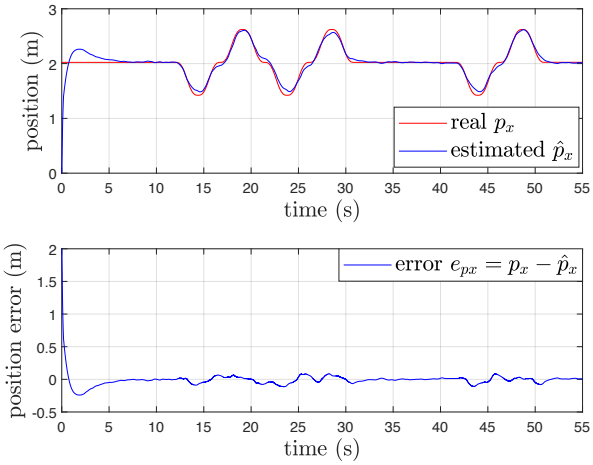

Fig. 10. Real and estimated position component p_x. Test with 4 anchors.

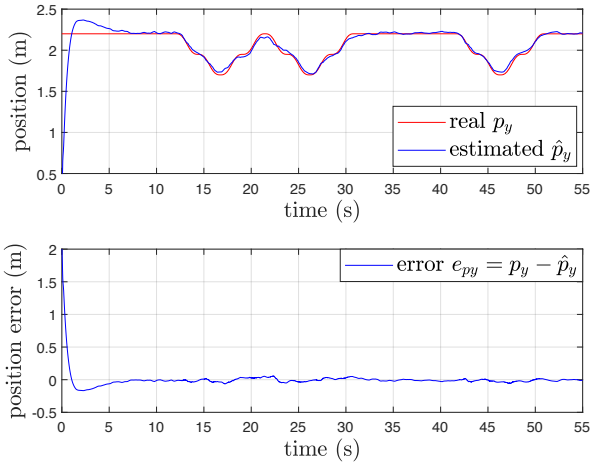

Fig. 11. Real and estimated position component p_y. Test with 4 anchors.

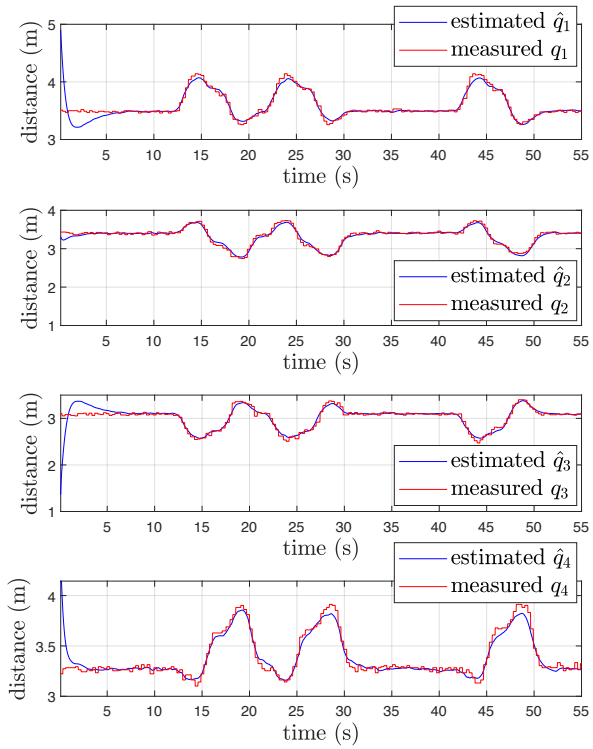

Fig. 12. Measured and estimated distances q_1,q_2 q_3 and q_4. Test with 4 anchors.

C. Comparison with general nonlinear least-square trilateration

In this subsection a comparison has been carried out between the proposed algorithm and the general Nonlinear Least-Squares (NLS) trilateration, based on Newton's method. In particular, the same experiment shown in the previous section has been done, with the same path and under same conditions, and the results are given in Figs. 15-16 and Tab. I. In particular, from Figs. 15-16 it is clear that the proposed algorithm exhibits a better filtering action and a smaller estimation error. On the contrary the general NLS trilateration method presents

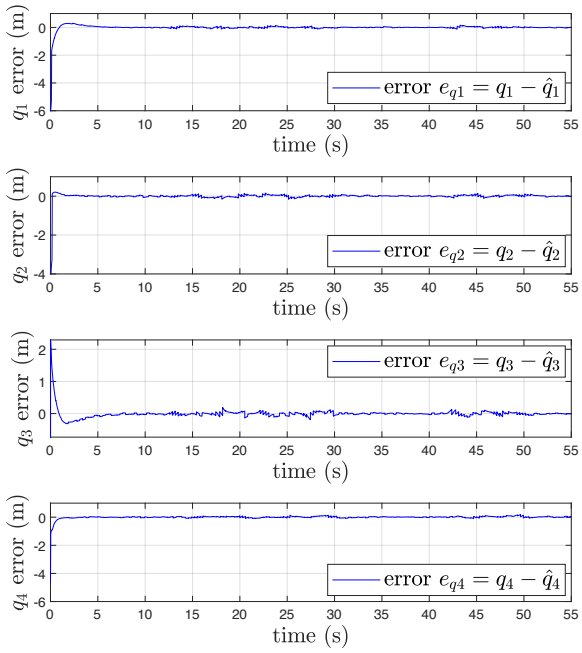

Fig. 13. Distance errors. Test with 4 anchors.

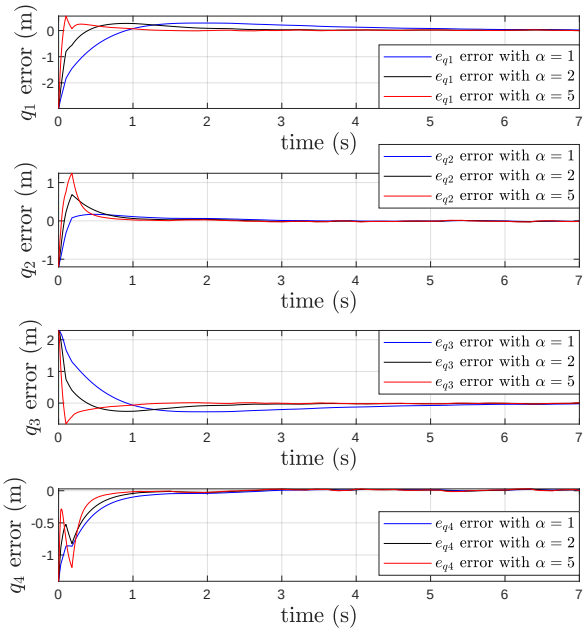

Fig. 14. Estimation error waveforms with different values of α. Test with 4 anchors.

a smaller settling time. However, the speed of convergence of the proposed algorithm is sufficiently high, and it can be possibly increased as shown in Prop. 1. Obviously, a higher convergence speed would results in a noisier estimate.

In order to quantify exactly the performances of the two algorithms the following indexes have been defined and their values are shown in Tab. I:

$$IAE_{SS} = \frac{1}{T_f - T_s} \int_{T_f}^{T_f} \sum_{k=x,y,z} |p_k(t) - \hat{p}_k(t)| dt \qquad (30)$$

TABLE I
PERFORMANCE INDEXES FOR LOW SPEED TEST

	Proposed algorithm	General NLS trilateration
IAE_{SS}	0.1062	0.1706
$ITAE$	1.34	2.86

TABLE II
PERFORMANCE INDEXES FOR HIGHER SPEED TEST

	Proposed algorithm	General NLS trilateration
IAE_{SS}	0.1245	0.1553
$ITAE$	1.88	2.79

$$ITAE = \frac{1}{T_f} \int_0^{T_f} t \left(\sum_{k=x,y,z} |p_k(t) - \hat{p}_k(t)| \right) dt \qquad (31)$$

where T_s is the settling time (in our case $T_s = 2.5$s), and T_f is the final time. In particular, the index IAE_{ss} represents the integral absolute error during steady state and the index $ITAE$ represents the integral time-weighed absolute error of the estimation error. As expected the two values of IAE_{ss} and $ITAE$ computed for the proposed algorithm are lower than the general NLS trilateration method (about -40% for IAE_{ss} and about -54% for $ITAE$).

In order to evaluate the performance with higher velocities and higher accelerations, a second test has been carried out, maintaining the same path, but with a higher velocity. The results of this second test are shown in Figs. 17-18 and Tab. II. Also in this case the same considerations already given above hold, indeed it is evident a better filtering action of the proposed technique. However, looking at Tab. II the margins of improvement are a little bit reduced due to a faster dynamics of the general NLS trilateration. In any case, the performance indexes with the proposed method are better than general NLS trilateration, indeed the IAE_{ss} is almost 20% less and the $ITAE$ is almost 33% less.

With regards to the computational complexity, the scheduling time for both algorithms has been computed. In particular, using a Raspberry Pi3, the following scheduling times have been obtained:

- 43 μs for the general NLS trilateration;
- 97 μs for the proposed algorithm.

This means that the maximum execution frequency that can be obtained with general NLS trilateration is about 23kHz, while with the proposed algorithm is about 10kHz. Even if the proposed algorithm is heavier from the computational effort point of view, 10kHz is much more higher than the required frequency for this kind of applications. Note that the real bottleneck is given by the UWB measurement frequency that, in our case, is 12Hz. Therefore, even if the two algorithms can be executed, potentially, with a very high frequency, they have to deal with a low measurement frequency.

D. Sensitivity analisys

Normally, the accuracy of the position estimate changes depending on different sensors and different positions. This is generally related with both the type of sensors and the algorithm used. In this section it is not investigated the

This article has been accepted for publication in a future issue of this journal, but has not been fully edited. Content may change prior to final publication. Citation information: DOI 10.1109/TIE.2021.3050354, IEEE Transactions on Industrial Electronics

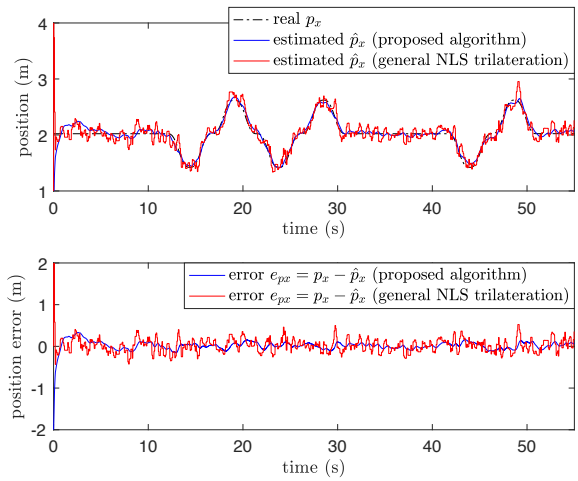

Fig. 15. Real and estimated position component p_x using both the proposed localization algorithm and a general NLS trilateration.

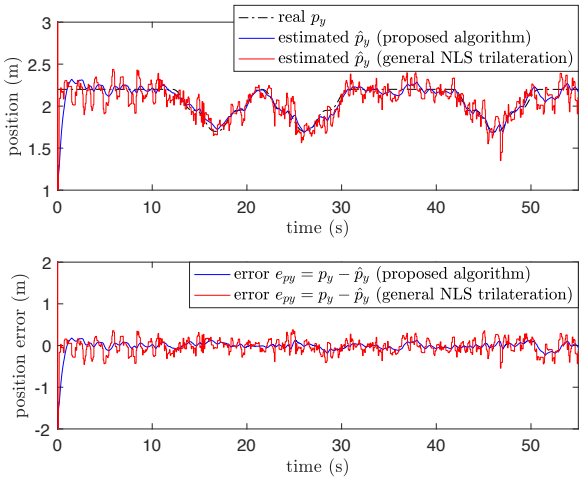

Fig. 16. Real and estimated position component p_y using both the proposed localization algorithm and a general NLS trilateration.

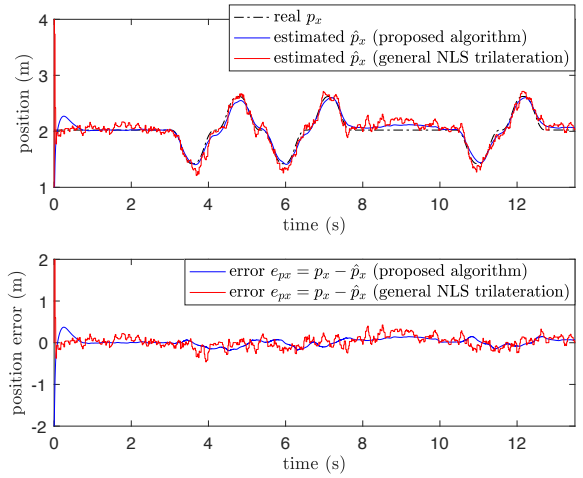

Fig. 17. Real and estimated position component p_x using both the proposed localization algorithm and a general NLS trilateration.

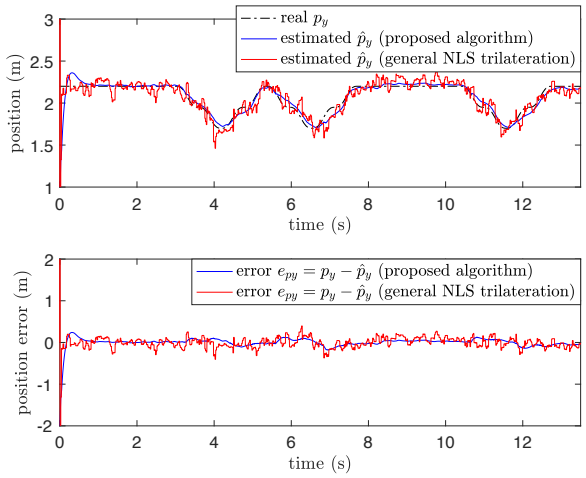

Fig. 18. Real and estimated position component p_y using both the proposed localization algorithm and a general NLS trilateration.

accuracy of the estimate related with the particular choice of a sensor, because it is not the main focus of the paper. Actually, it does not depend to the algorithm, but it depends to the experimental set-up. However, an analysis will be carried out in order to give some hints about the sensitivity of the proposed algorithm with respect to different positions and different number of anchors. In particular, the inverse on the norms of matrices $\mathbf{J}^{-1}_{\mathcal{K}^{-1}}(\mathbf{p})$ (for the case with three anchors) and $\mathbf{J}^{\#}_{\mathcal{K}^{-1}}(\mathbf{p})$ (for the case with four anchors) are used to define the *mean sensitivity* indexes of the algorithm as follows:

$$\mathcal{S}_3 = ||\mathbf{J}^{-1}_{\mathcal{K}^{-1}}||^{-1}_2, \quad \mathcal{S}_4 = ||\mathbf{J}^{\#}_{\mathcal{K}^{-1}}||^{-1}_2. \tag{32}$$

The indexes $\mathcal{S}_3$ and $\mathcal{S}_4$ can be effectively considered as a kind of *"sensitivity"* for the proposed algorithm because matrices $\mathbf{J}^{-1}_{\mathcal{K}^{-1}}(\mathbf{p})$ and $\mathbf{J}^{\#}_{\mathcal{K}^{-1}}(\mathbf{p})$ represent how the distance measurement errors are transferred to the position estimate derivative $\dot{\mathbf{p}}$. Lower these indexes are, higher (on average) the position estimate derivative is. Consequently, possible errors on the measurements result in high errors on the estimate if the indexes $\mathcal{S}_3$ and $\mathcal{S}_4$ are very small.

The values of $\mathcal{S}_3$ and $\mathcal{S}_4$ are computed and the results are shown in Figs. 19-20. In particular, Fig. 19 represents the case with three anchors, and it shows the value of $\mathcal{S}_3$, as defined in (32), for different values of x and y coordinates considering four values of z coordinate: $z = 0.6$m, $z = 1.2$m, $z = 1.8$m and $z = 2.4$m. While Fig. 20 represents the same type of surfaces, but for the case with four anchors. From these figures it is evident a lower sensitivity of the estimate when the point P is close to the anchors. Note that when the point P coincides with one of the anchors the indexes $\mathcal{S}_3$ and $\mathcal{S}_4$ are not defined (See comment after Eq. (9)). However, as already said, this last condition is not realistic from a practical point of view. Another important consideration, coming from the analysis of Fig. 19, is that for some points the value of $\mathcal{S}_3$ is zero. These points coincide with the intersection of the Σ_A plane containing the anchor A_1, A_2 and A_3, and the horizontal plane with a constant value of z. In this line there is a singularity as expected, and this is the reason why the Assumption 1 is

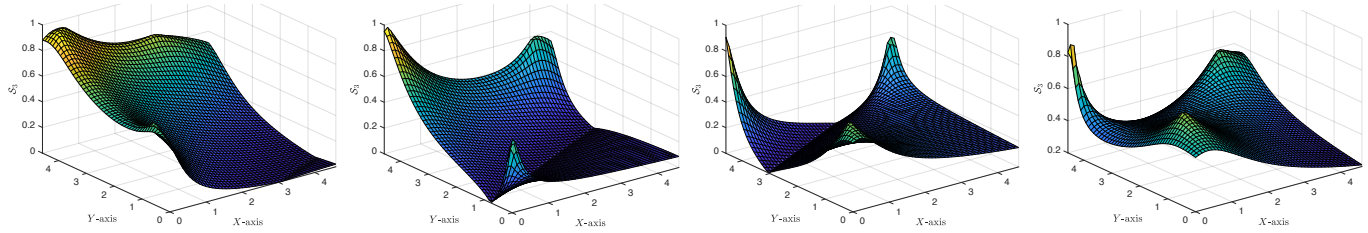

(a) (b) (c) (d)

Fig. 19. Mean sensitivity $\mathcal{S}$, using three anchors, for: $z = 0.6$m (a), $z = 1.2$m (b), $z = 1.8$m (c) and $z = 2.4$m (d).

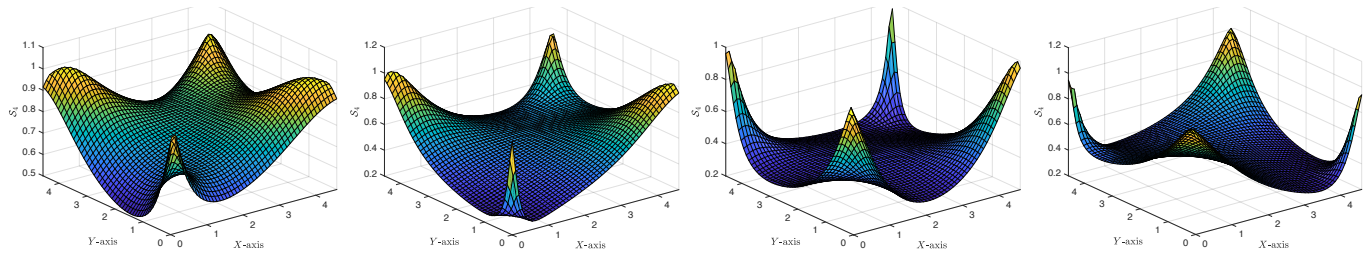

(a) (b) (c) (d)

Fig. 20. Mean sensitivity $\mathcal{S}$, using four anchors, for: $z = 0.6$m (a), $z = 1.2$m (b), $z = 1.8$m (c) and $z = 2.4$m (d).

necessary for the case of three anchors. Obviously, there is not this problem if four anchors are used as shown in Fig. 20.

VI. Conclusions

In this work a new scheme for a range-based localization system has been given. The proposed approach is very suitable for applications in which the GPS fails, like indoor or urban environments. It has been shown that the method based on the direct kinematics problem for parallel robot is very appealing because: a) it is a deterministic method, easily understandable and easy to implement; b) it is an iterative method based on a closed loop control scheme; c) it is possible to prove the exponential convergence to zero of the estimation error as well as an explicit tuning rule to ensure a well defined convergence speed. In particular, the possibility to fix a-priori the convergence speed of the estimation error represents an appealing result from the practical point of view compared with existing methods proposed in literature based on trilateration, where these types of theoretical certificates cannot be given. Finally, the effectiveness of the proposed approach has been proven by means of experimental results.

References

[1] T. Hamel and R. Mahony, "Attitude estimation on SO(3) based on direct inertial measurements," in *IEEE International Conference on Robotics and Automation*. Orlando, United States: IEEE, 2006, pp. 2170–2175.

[2] T. I. Fossen, *Handbook of marine craft hydrodynamics and motion control*. John Wiley & Sons, 2011.

[3] W. Zhang, M. Ghogho, and B. Yuan, "Mathematical model and matlab simulation of strapdown inertial navigation system," *Modelling and Simulation in Engineering*, vol. 2012, pp. 1–25, 2012.

[4] A. Amanatiadis, "A multisensor indoor localization system for biped robots operating in industrial environments," *IEEE Transactions on Industrial Electronics*, vol. 63, no. 12, pp. 7597–7606, 2016.

[5] W. Chen, J. Xu, X. Zhao, Y. Liu, and J. Yang, "Separated sonar localization system for indoor robot navigation," *IEEE Transactions on Industrial Electronics*, 2020.

[6] T. I. Fossen, *Guidance and control of ocean vehicles*. John Wiley & Sons, 1994.

[7] ——, *Marine Control Systems: Guidance, Navigation and Control of Ships, Rigs and Underwater Vehicles*. Marine Cybernetics, Trondheim, Norway, 2002.

[8] L. Paull, S. Saeedi, M. Seto, and H. Li, "AUV navigation and localization: A review," *IEEE Journal of Oceanic Engineering*, vol. 39, no. 1, pp. 131–149, 2014.

[9] O. J. Woodman, "An introduction to inertial navigation," University of Cambridge, Computer Laboratory, Tech. Rep., 2007.

[10] H. F. Grip, T. Fossen, T. A. Johansen, and A. Saberi, "Nonlinear observer for GNSS-aided inertial navigation with quaternion-based attitude estimation," in *IEEE American Control Conference*. Washington DC, United States: IEEE, 2013, pp. 272–279.

[11] B. Liu, S. Wei, J. Lu, J. Wang, and G. Su, "Fast self-alignment technology for hybrid inertial navigation systems based on a new two-position analytic method," *IEEE Transactions on Industrial Electronics*, vol. 67, no. 4, pp. 3226–3235, 2019.

[12] F. Alonge, F. D'Ippolito, G. Garraffa, and A. Sferlazza, "A hybrid observer for localization of mobile vehicles with asynchronous measurements," *Asian Journal of Control*, vol. 21, no. 4, pp. 1506–1521, 2019.

[13] K. Guo, Z. Qiu, C. Miao, A. H. Zaini, C.-L. Chen, W. Meng, and L. Xie, "Ultra-wideband-based localization for quadcopter navigation," *Unmanned Systems*, vol. 4, no. 1, pp. 23–34, 2016.

[14] A. Yassin, Y. Nasser, M. Awad, A. Al-Dubai, R. Liu, C. Yuen, R. Raulefs, and E. Aboutanios, "Recent advances in indoor localization: A survey on theoretical approaches and applications," *IEEE Communications Surveys & Tutorials*, vol. 19, no. 2, pp. 1327–1346, 2016.

[15] F. Zafari, A. Gkelias, and K. K. Leung, "A survey of indoor localization systems and technologies," *IEEE Communications Surveys & Tutorials*, vol. 21, no. 3, pp. 2568–2599, 2019.

[16] F. Alonge, F. D'Ippolito, G. Garraffa, and A. Sferlazza, "Hybrid observer for indoor localization with random time-of-arrival measurments," in *International Forum on Research and Technology for Society and Industry*. Palermo, Italy: IEEE, 2018, pp. 1–6.

[17] S. Promwong and P. Southisombat, "UWB transmission measurement and modeling for indoor localization," in *International Computer Science and Engineering Conference*. Chiangmai, Thailand: IEEE, 2016, pp. 1–4.

[18] N. Gutierrez, C. Belmonte, J. Hanvey, R. Espejo, and Z. Dong, "Indoor localization for mobile devices," in *International Conference on Networking, Sensing and Control*. Miami, FL, USA: IEEE, 2014, pp. 173–178.

[19] W. Murphy and W. Hereman, "Determination of a position in three dimensions using trilateration and approximate distances," *Department*

of Mathematical and Computer Sciences, Colorado School of Mines, Golden, Colorado, vol. 7, pp. 1–19, 1995.
[20] D. E. Manolakis, "Efficient solution and performance analysis of 3-D position estimation by trilateration," *IEEE Transactions on Aerospace and Electronic systems*, vol. 32, no. 4, pp. 1239–1248, 1996.
[21] W. Navidi, W. S. Murphy Jr, and W. Hereman, "Statistical methods in surveying by trilateration," *Computational statistics & data analysis*, vol. 27, no. 2, pp. 209–227, 1998.
[22] B. Siciliano, "The tricept robot: Inverse kinematics, manipulability analysis and closed-loop direct kinematics algorithm," *Robotica*, vol. 17, no. 4, pp. 437–445, 1999.
[23] H. Nourmohammadi and J. Keighobadi, "Design and experimental evaluation of indirect centralized and direct decentralized integration scheme for low-cost INS/GNSS system," *GPS Solutions*, vol. 22, no. 3, p. 65, 2018.
[24] P. Doostdar and J. Keighobadi, "Design and implementation of SMO for a nonlinear MIMO AHRS," *Mechanical Systems and Signal Processing*, vol. 32, pp. 94–115, 2012.
[25] J. Keighobadi, M. Hosseini-Pishrobat, J. Faraji, and M. N. Langehbiz, "Design and experimental evaluation of immersion and invariance observer for low-cost attitude-heading reference system," *IEEE Transactions on Industrial Electronics*, vol. 67, no. 9, pp. 7871–7878, 2019.
[26] P. Doostdar, J. Keighobadi, and M. A. Hamed, "INS/GNSS integration using recurrent fuzzy wavelet neural networks," *GPS Solutions*, vol. 24, no. 1, p. 29, 2020.
[27] B. Siciliano, L. Sciavicco, L. Villani, and G. Oriolo, *Robotics: modelling, planning and control*. Springer Science & Business Media, 2010.
[28] J. P. Hespanha, *Linear systems theory*. Princeton university press, 2018.
[29] J. Lofberg, "YALMIP: A toolbox for modeling and optimization in MATLAB," in *IEEE international conference on robotics and automation*. New Orleans, LA, USA: IEEE, 2004, pp. 284–289.
[30] I. Frosio, F. Pedersini, and N. A. Borghese, "Autocalibration of MEMS accelerometers," *IEEE Transactions on Instrumentation and Measurement*, vol. 58, no. 6, pp. 2034–2041, 2008.
[31] C. Chi, J.-W. Lv, and D. Wang, "Calibration of triaxial magnetometer with ellipsoid fitting method," in *IOP Conf. Series: Earth and Environmental Science*, vol. 237, no. 3. IOP Publishing, 2019, pp. 1–6.
[32] S. Madgwick, "An efficient orientation filter for inertial and inertial/magnetic sensor arrays," *Report x-io and University of Bristol (UK)*, vol. 25, pp. 113–118, 2010.

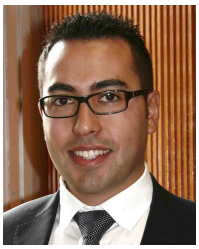

Antonino Sferlazza (S'12–M'15) was born in Palermo, Italy, in 1987. He received the Master degree in automation engineering and the Ph.D. degree in mathematics and automation from the University of Palermo, Italy, in 2011 and 2015 respectively. In 2013 he was visiting PhD student at University of California at Santa Barbara, CA, USA. From 2016 to 2017 he join the University of Palermo as junior researcher. From 2017 to 2018 he was researcher are LAAS CNRS of Toulouse, France. He is currently a researcher in systems and control engineering at the University of Palermo. His research interests include the development of feedback control algorithms for nonlinear dynamical systems, estimation theory, and applications of control of electrical drives, power converters, and mechanical systems.

Giovanni Garraffa was born in Palermo, Italy, in May 1986. He received the Master's degree in automation engineering from the University of Palermo, Palermo, Italy. Currently he is PhD student in "Energy and Information Technology Engineering" at the University of Palermo, Palermo, Italy. His research interests include the development of algorithms for indoor vehicles localization and autonomous flight. He is also interested on the development of testing platform to evaluate control algorithm performances.

Filippo D'Ippolito (M'00) was born in Palermo, Italy, in 1966. He received the Laurea degree in Electronic Engineering from the University of Palermo in 1991. He received the Research Doctorate degree in Systems and Control Engineering from the University of Palermo in 1996. He is currently a Research Associate in the Department of Systems and Control Engineering at the University of Palermo. His research interests include control of electrical drives, control of electrical power converters, adaptive and visual/force control of robot manipulators, rehabilitation robotics, marine robotics. Dr. D'Ippolito received the 2000 Kelvin Premium from the Institution of Electrical Engineers (IEE), for the paper "Parameter identification of induction motor model using genetic algorithms".

Francesco Alonge (M'02–SM'19) was born in Agrigento, Italy, in 1946. He received the Laurea degree in electronic engineering from the University of Palermo in 1972. Since then, he has been with the University of Palermo, where he is currently a full Professor of Automatic Control in the Department of Systems and Control Engineering. His research topics include electrical drive control (including also linear and nonlinear observers, stochastic observers, parametric identification), robot control, parametric identification and control in power electronics, UAV motion control in aeronautics.